Definable Equilibrium States in the Folding of Human Prion Protein†

Laszlo L. P. Hosszu,*,‡,§ Mark A. Wells,‡,§ Graham S. Jackson,‡ Samantha Jones,‡ Mark Batchelor,‡ Anthony R. Clarke,‡,|| C. Jeremy Craven,§ Jonathan P. Waltho,§ and John Collinge‡

MRC Prion Unit and National Prion Clinic, Institute of Neurology and National Hospital for Neurology and Neurosurgery, Queen Square, London WC1N 3BG, U.K., Krebs Institute for Biomolecular Research, Department of Molecular Biology and Biotechnology, University of Sheffield, Sheffield S10 2TN, U.K., and Department of Biochemistry, School of Medical Sciences, University of Bristol, Bristol BS8 1TD, U.K.

Received July 4, 2005; Revised Manuscript Received October 24, 2005

ABSTRACT: The role of conformational intermediates in the conversion of prion protein from its normal cellular form (PrP^C) to the disease-associated "scrapie" form (PrP^{Sc}) remains unknown. To look for such intermediates in equilibrium conditions, we have examined the unfolding transitions of PrP^C, primarily using the chemical denaturant guanidine hydrochloride (GuHCl). When the protein conformation is assessed by NMR, there is a gradual shift of NMR signals in the regions between residues 125−146 and 186−196. The denaturant dependence of these shifts shows that in aqueous solution the native and locally unfolded conformations are both significantly populated. Following this shift, there is the major unfolding transition to generate a substantially unfolded population. However, analysis of NMR chemical shift and intensity changes shows that there is persistent structure in the molecule well beyond this major cooperative unfolding transition. Residual structure within this state is extensive and encompasses the majority of the secondary structure elements found in the native state of the protein.

Prion diseases are fatal neurological diseases associated with the deposition of host-encoded prion protein (PrP)[1] in aggregates which may form amyloid fibrils (*1*). This disease-associated form of the protein, termed the scrapie form, or PrP^{Sc}, differs from the normal cellular form (PrP^C) through a conformational change, resulting in a significant increase in the β-sheet content and protease resistance of the protein (*2*−*4*). No covalent modifications between the two isoforms have been consistently identified to date. According to the protein-only hypothesis (*5*), the infectious agent is composed of a conformational isomer of prion protein (*6*) that is able to convert other isoforms to the infectious isomer in an autocatalytic manner. The most coherent and general model proposed thus far is that PrP^C fluctuates between the dominant native state and minor conformations, one or a set of which can self-associate in an ordered manner to produce a stable supramolecular structure composed of misfolded PrP monomers.

Amyloid formation in a number of proteins is associated with destabilization of the native protein through somatic mutations, increasing the steady-state concentration not only of the unfolded state but also of partially folded intermediate states (*7*−*10*). In the case of PrP, although no definite link between PrP^C stability and disease has been established, all fully penetrant pathogenic mutations show significant destabilization, whereas nonpathogenic mutations do not (*11*). Further, in vitro experiments have shown that destabilization of the native state of prion through the use of chemical denaturants, or DNA-binding, also favors the formation of protease-resistant and/or fibrillar conformations (*12*−*14*), some of which have been claimed to be associated with the disease process (*13*). Numerous studies have therefore been undertaken in order to identify and characterize non-PrP^C conformers of PrP, under both equilibrium and kinetic conditions. PrP^C has a largely α-helical conformation (*15*, *16*), for which the urea denaturation is well described by a two-state equilibrium between folded and denatured states (*13*). However, PrP^C can be converted to a variety of other, intermediate, conformations, usually with enhanced β-sheet content, by changing the pH, temperature, and/or redox conditions (*17*−*19*), several of which appear to be associated with oligomerization of non-native forms of the protein (*13*, *20*, *21*).

In terms of monomeric intermediate states, hydrogen exchange data support a model where the core of PrP^C, encompassing the three main α-helices and second β-strand of the protein, is a stable block, exhibiting protection from exchange at least equivalent to the equilibrium constant between the folded and denatured forms of the protein (*22*). However, part of this core remains as a residual, hyperstable region within the denatured form, consisting of at least 10 residues centered on the disulfide bond linking helices II and III. An analogous hyperstable region is not present in the PrP homologue, doppel (*23*), or indeed in most other

† This work was funded by the Medical Research Council.

* Corresponding author. Tel: +44 114 222 2717. Fax: +44 114 222 2800. E-mail: l.l.hosszu@shef.ac.uk.

‡ Institute of Neurology and National Hospital for Neurology and Neurosurgery.

§ University of Sheffield.

|| University of Bristol.

[1] Abbreviations: CD, circular dichroism; PrP, prion protein; PrP^C, cellular PrP isoform; PrP^{Sc}, pathogenic (scrapie) PrP isoform; PrP^{91-231}, human prion protein (residues 91−231); EDTA, ethylenediaminetetraacetic acid; GuHCl, guanidine hydrochloride; HSQC, heteronuclear single-quantum coherence; SEC, size exclusion chromatography; TSP, sodium 3-(trimethylsilyl)-[2,2,3,3-$^2H_4$]propionate; 2D, two dimensional, 3D, three dimensional.

10.1021/bi051277k CCC: $30.25
Published on Web 11/22/2005

disulfide-bonded proteins studied to date (*24*−*26*). These data indicate that routes to form intermediate states involving regions outside of this hyperstable core region should be favored over those that require the core of the protein to be disrupted. An inherent limitation of the hydrogen exchange technique, however, is that it only provides information for those regions in proteins which otherwise display measurable protection from exchange from the folded form. Typically, these are regions that are structured within the folded state. The implication of this is that the extent of any intermediate state found within PrP may be severely underestimated and biased toward secondary structure elements.

To characterize more fully the conformational possibilities available to PrP, its behavior as a function of the chemical denaturant guanidine hydrochloride (GuHCl) was monitored. Recently, variable behavior of both the native and denatured states as a function of urea concentration has been reported, where the dimensions of each species increased with increasing denaturant concentration (*13*). Here we analyze the conformational heterogeneity underlying these changes within both the folded and the denatured state ensembles, primarily using heteronuclear NMR methods. The folded state ensemble shows evidence of fraying of the C-termini of helices II and III, and a perturbation of the loop connecting these helices, with chemical shift data consistent with the N-terminal region of the folded domain (residues 125−146) spending a proportion of time detached from the folded core of the protein. The denatured state ensemble contains a so-called pre-molten globule component (*27*), which encompasses many of the residues corresponding to the folded C-terminal domain of PrP^C and which is considerably larger than the hyperstable core surrounding the disulfide bond identified by hydrogen exchange. This state is distinct from previously described monomeric intermediates, which are essentially perturbations of the native state conformation rather than largely unfolded species. Similar denaturing conditions have been used to generate prion protein fibrils and putative synthetic prion infectivity (*13*). In other proteins, such pre-molten globule states have been proposed previously to be important in amyloid and fibril formation (*27*).

MATERIALS AND METHODS

Protein Expression, Purification, and Preparation. The protein construct used in this study comprises residues 91−231 of human prion protein (PrP^{91-231}). Expression and purification of ^{15}N- and $^{13}C/^{15}N$-labeled protein for NMR study were carried out as described previously (*16*). Samples were stored in 6 M GuHCl concentration and 100 mM EDTA, pH 8.0 at −20 °C, prior to use. Protein samples for the backbone assignment of the unfolded state of PrP were buffer-exchanged by repeated concentration/dilution in Amicon 50 pressure cells into 20 mM sodium acetate-d_3 and 3 mM sodium azide, pH 5.55 [10% D_2O (v/v)], containing 4 M GuHCl concentration. Protein concentrations were 0.6−1.2 mM.

NMR Spectroscopy. NMR spectra were acquired at 298 K on Bruker DRX-600 and DRX-800 spectrometers equipped with 5 mm $^{13}C/^{15}N/^1H$ triple-resonance probes. Proton chemical shifts were referenced to 1 mM TSP added to the samples. ^{15}N and ^{13}C chemical shifts were calculated relative to TSP, using the gyromagnetic ratios of ^{15}N, ^{13}C, and ^1H ($^{15}N/^1H = 0.101329118$, $^{13}C/^1H = 0.25144953$). NMR data were processed and analyzed on Silicon Graphics and Linux Workstations using Felix 2000 (Accelrys, San Diego, CA) and NMRview software (*28*).

Backbone Resonance Assignments of the Unfolded States of Prion Protein. Backbone resonance assignments were achieved using the standard suite of triple-resonance experiments [HNCO, HN(CA)CO, HNCACB, CBCA(CO)NH] (*29*−*32*). Peak picking was performed semimanually. The backbone assignment methodology used the "asstools" set of assignment programs (*33*). The default option and values within the program were used, with the standard table of C^α and C^β chemical shifts replaced with a table containing ranges 0.5 ppm from random coil values. Sequential assignments were achieved mainly through linking of preceding and intraresidue carbonyl chemical shifts, as the long $^{13}C'$ and ^{15}N T_2 relaxation times allowed long $^{13}C'$ (180 ms) and ^{15}N (69 ms) acquisition times, giving good resolution in these dimensions in the HNCO and HN(CA)CO spectra. C^α and C^β matches were used mainly for residue type and preceding residue-type identification.

GuHCl Titration of Prion Protein Monitored by NMR Spectroscopy. A 1.1 mM sample of ^{15}N-labeled PrP in 20 mM sodium acetate, 3 mM sodium azide, and 1 mM TSP, pH 5.5 [10% D_2O (v/v)], was titrated with aliquots of 8 M GuHCl in the same buffer to a final concentration of 6.4 M GuHCl. Following each addition of denaturant, the sample was allowed to equilibrate for 60 min at 298 K before being placed in the magnet. The 1D ^1H and 2D $^1H-^{15}N$ HSQC spectra were acquired at the same temperature. The $^1H-^{15}N$ HSQC spectra were acquired using sensitivity-enhanced pulsed field gradient coherence selection (*34*, *35*) with acquisition times of 138 and 87.5 ms in the ^1H and ^{15}N dimensions, respectively. The intensities of resolved HSQC resonances were measured and normalized to the intensity of the backbone resonance of residue A117, whose intensity remained approximately constant throughout the titration.

Calculation of Denaturant Activity. Due to the nonlinear relationship between denaturant concentration and the free energy for folding, GuHCl concentration ([GuHCl]) is converted to molar denaturant activity to obtain a more reliable extrapolation of data at high denaturant concentrations. The equation used is

$$D = [\text{GuHCl}](7.5\ \text{M}/(7.5\ \text{M} + [\text{GuHCl}]))$$

(*36*), where D is the molar denaturant activity. In this paper, denaturant activities will be used, with the corresponding denaturant concentrations following within square brackets.

pH Titration of Prion Protein Monitored by NMR Spectroscopy. The pH titration of PrP^C was carried out in an analogous manner to the GuHCl titration, with a 1 mM ^{15}N-labeled PrP^C sample titrated with 0.1 M HCl, from an initial pH of 5.5 to a final pH of 3.85.

Equilibrium Denaturation Data Monitored by CD. The amide CD absorption of 7 μM PrP^{91-231} in 20 mM sodium acetate-d_3 and 2 mM sodium azide, pH 5.55, was recorded in varying concentrations of GuHCl as previously described (*16*, *22*). The ellipticity signal (α) was converted to the proportion of molecules in the native state α_N according to the relationship $\alpha_N = (\theta - \theta_U)/(\theta_N - \theta_U)$, where θ_U and θ_N are the ellipticity signals for the unfolded and native states,

respectively. Data were fitted to the function:

$$\alpha_N = [K(\mathrm{N/U})\exp(mD)]/[1 + K(\mathrm{N/U})]$$

where m represents the sensitivity of the unfolding transition to denaturant and D is the denaturant activity (*36*).

RESULTS

The equilibrium denaturation of PrP^{91-231} as a function of guanidine hydrochloride (GuHCl) concentration was monitored using a combination of NMR and CD spectroscopy. A selection of 1D ^1H NMR spectra is shown in Figure 1a. As denaturant is added, loss of chemical shift dispersion, characteristic of loss of specific tertiary structure, is observed. This loss occurs in a largely cooperative manner, with a midpoint of approximately 1.5 M GuHCl activity ([~1.9 M GuHCl]; see Materials and Methods), and corresponds well with the major unfolding transition, as monitored by far-UV (amide) circular dichroism (far-UV CD) (Figure 1b). These data are consistent with previous chemical denaturant studies of PrP (*13*) and, to a first approximation, can be described by a two-state unfolding transition; i.e., no resolvable population of intermediate states with conformations largely dissimilar from either the native or the denatured states is observed. By 1.9 M GuHCl activity ([~2.5 M GuHCl]), almost complete loss of chemical shift dispersion is observed in the NMR spectra, indicating that the protein is predominantly unfolded. However, outside of the transition region, both the folded and the denatured states show nonuniform behavior as a function of GuHCl concentration, consistent with their nonuniform dimensions as a function of urea (*13*), and are more accurately described as native and denatured state ensembles.

Perturbation of the Native State Ensemble. Some change in the nature of the folded state ensemble prior to the major unfolding transition is revealed by the substantial pretransition baseline slope seen in the far-UV CD signal (Figure 1b), similar to that reported previously for urea (*13*). Inspection of the ^1H NMR chemical shifts prior to the unfolding transition region reveals marked changes as a function of denaturant concentration. For example, the proton resonances corresponding to I139 H^δ and I182 H^γ (Figure 1a) shift substantially prior to unfolding, indicating that the tertiary structure surrounding these residues is being disturbed. Using 2D $^1H-^{15}N$ HSQC spectra, the regions where denaturant-induced changes in conformation within the native state ensemble occur can be mapped onto the tertiary structure. Although the large majority of peaks exhibit little change in chemical shift prior to unfolding, a distinct subset of resonances within the protein are subject to a GuHCl-dependent effect at low GuHCl concentrations (Figure 2 a,b). It is possible to follow the movement in peaks, as the conformational transitions that are taking place in the protein are fast relative to the NMR chemical shift changes, leading to the averaging of the NMR signals (the fast exchange regime). The chemical shift movements at low denaturant concentration are localized in three main regions, the N-terminus of the folded domain up to the N-terminus of helix I (residues 125−146), the C-terminus of helix II and the loop linking it to helix III (residues 182, 186−196), and the C-terminus of helix III (residues 220−229) (Figure 2a,b). Although the chemical shift changes at the C-terminus of helix III show some correlation with those seen in the major unfolding transition (Figure 3 c), indicating that the direction of the conformational shift for this region of the protein is the same as the major unfolding transition, the majority of shift changes are not due to the native-to-unfolded state transition, since there is no strong correlation between the ^{15}N chemical shift changes observed on addition of low concentrations of GuHCl with those observed upon unfolding (Figure 3c). This indicates that the changes observed at low denaturant are not due to a simple two-state transition from the folded to unfolded state. In addition, they are not due to some form of multimerization, as no discernible differences in chemical shift changes are observed at reduced (500 μM) protein concentration.

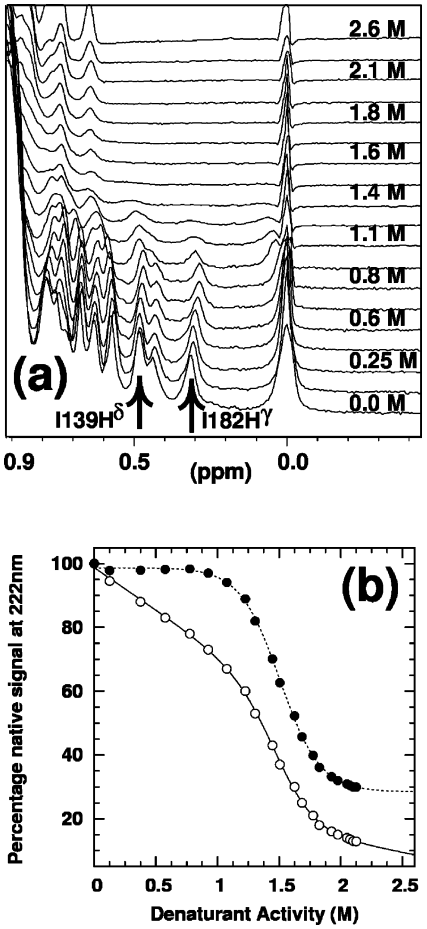

FIGURE 1: Equilibrium denaturation of PrP^{91-231}. Shown in (a) is the upfield-shifted methyl region of 1D NMR spectra at increasing GuHCl activities. Movement of NMR peaks prior to the major unfolding transition, for example, I139 H^δ and I182 H^γ, indicates changes in the tertiary structure of the PrP^c native state ensemble. In contrast, intensity and chemical shift changes at elevated denaturant activities (>1.5 M GuHCl) ([>1.9 M GuHCl]; see Materials and Methods) indicate changes in the denatured state ensemble. Shown in (b) is the equilibrium unfolding profile monitored by far-UV circular dichroism (open circles). The solid line represents the nonlinear least-squares fit to a model with pre- and post-transition baseline slopes, with the dotted line representing the same two-state model with the pre- and post-transition baselines removed. The solid circles show data points corrected for the pre- and post-transition baselines.

Comparison of Low-Denaturant and Acid pH States. The GuHCl-induced changes in chemical shift within the native state ensemble mirror closely, in both distribution and amplitude, a number of the changes observed upon acidifica-

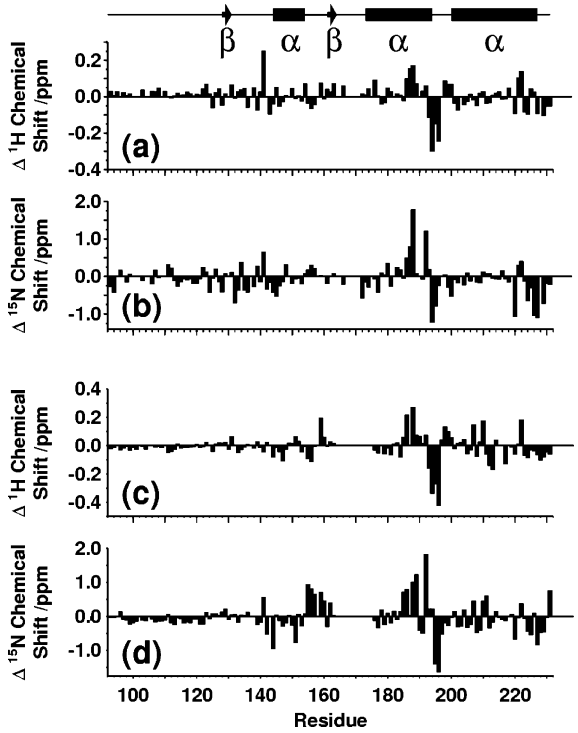

FIGURE 2: Chemical shift changes in the prion protein native state ensemble prior to the major unfolding transition. (a, b) Effect of GuHCl. Chemical shift (^{1}H and ^{15}N) changes between 0 and 0.95 M GuHCl activity ([0.0−1.1 M GuHCl]). In this and following figures, secondary structure elements of the PrP^C native state are drawn with α-helices represented by cylinders and the β-sheets by arrows (*16*). (c, d) Effect of acidification on the prion protein native state. Chemical shift (^{1}H and ^{15}N) changes upon reduction of pH from 5.5 to 3.9.

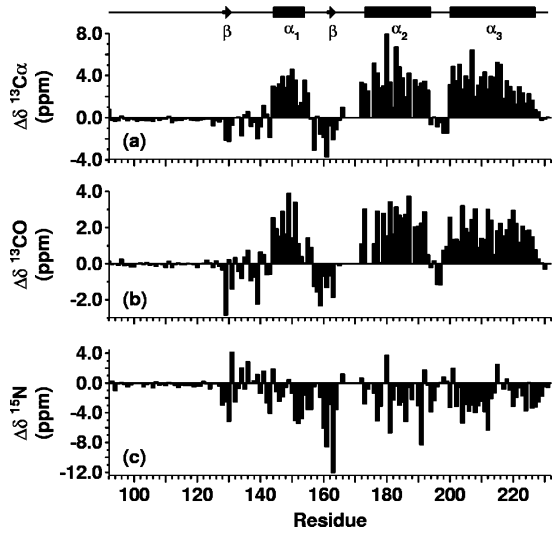

FIGURE 3: Chemical shift differences ($\Delta\delta$) of backbone resonances between the prion protein native state ensemble and the denatured state ensemble at 2.6 M GuHCl activity ([4.0 M GuHCl]). (a−c) C^α, carbonyl (CO), and ^{15}N (amide) chemical shift changes, respectively. The ^{13}C nuclei show a very strong correlation between carbon chemical shift and native state secondary structure elements.

tion of the protein from pH 5.5 to pH 3.9 (Figure 2c,d). Upon acidification, chemical shift changes occur for residues within the N-terminus of helix I and the C-termini of helices I, II, and III. The similarity in behavior between acidification- and GuHCl-induced chemical shift changes is most apparent around the C-termini of helices II and III, where the largest GuHCl-induced chemical shift movements occur. A comparison of the solution structure of HuPrP at pH 7.0 with that at pH 4.5 found that the pH-induced chemical shift changes correlated with relatively minor, and strictly localized, conformational differences (*37*), mainly associated with the fraying of helices at acidic pH. By analogy, it appears that the addition of GuHCl is also causing a perturbation of the C-termini of helices II and III, prior to the global unfolding transition, and that these chemical shift changes are reflecting a local perturbation of structure rather than the formation of a grossly perturbed intermediate state.

The region adjacent to the C-terminus of helix II provides the hinge in a 3D domain-swapped dimer of HuPrP (*38*), which often reflects some localized conformational strain within the monomeric state that is released on formation of the dimer (*39*, *40*). However, in HuPrP, domain swapping is also associated with intermolecular disulfide formation, using cysteine residues on either side of the hinge region, which complicates any analysis of the driving force for the reaction.

Perturbation of the 125−146 Region. The acidification- and the GuHCl-induced chemical shift changes correlate less well in the N-terminal region of the folded domain (residues 125−146), where the GuHCl-induced changes are widespread, indicative of a significant perturbation of this entire region. Size exclusion chromatography (SEC) and light scattering experiments indicate that the native state increases in volume as it approaches the denaturant-induced unfolding transition (*13*) or as the pH is reduced (*41*). However, the magnitudes of the ^{15}N chemical shift changes observed here prior to unfolding are on average only approximately 10% of those expected on denaturation (Figure 3c). This suggests that full detachment or unfolding of these regions from the remainder of the protein is not occurring. Hence, given the molecular volume measurements, species within the native state ensemble where residues 125−146 or the C-termini of helices II/III are perturbed must be significantly expanded, since the small magnitude of the chemical shift changes suggests they are only populated for a few percent of the time. Hence, chemical shift data suggest that the native state ensemble is likely to contain a population of conformers where parts of the folded domain become detached from the core region. This view is supported by the sensitivity of these regions to high hydrostatic pressure and by implication to volume changes (*42*, *43*). Further, hydrogen exchange data show that each of these regions is largely unprotected from solvent exchange, even in the absence of denaturant (*22*, *23*). The N-terminal region of the folded domain contains strand I of the β-sheet (residues 129−131). The second strand of the β-sheet (residues 160−164) has measurable hydrogen exchange protection factors. Rationalization of the hydrogen exchange, chemical shift, and SEC data leads to two possibilities: first, that the β-sheet is maintained at low denaturant concentrations and the loop region (residues 125−128, 132−145) detaches, or second, that the residues involved in hydrogen bonding within the β-sheet are involved in hydrogen bonding with other hydrogen bond acceptors.

The apparent absence of sigmoidal behavior in the transition observed at low denaturant concentrations indicates that the free energy and *m*-value changes associated with these perturbations are relatively small; however, the difficulty in estimating the signal for the fully folded state

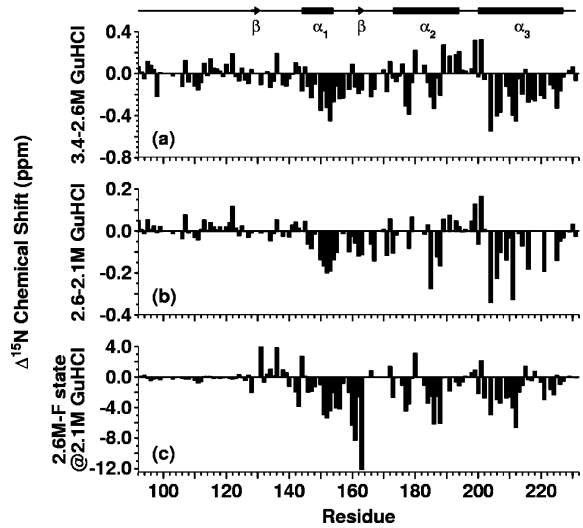

FIGURE 4: ^{15}N chemical shift changes within the denatured state ensemble of prion protein. Chemical shift changes between (a) 3.4−2.6 M GuHCl activity ([6.4−3.9 M GuHCl]) and (b) 2.6−2.1 M GuHCl activity ([3.9−3.0 M GuHCl]). Approximately 32 residues were unobservable at 2.1 M GuHCl activity because of line broadening of resonances caused by conformational fluctuations in the denatured state ensemble, precluding measurement of data. (c) shows ^{15}N chemical shift differences between the denatured state ensemble at 2.6 M GuHCl activity and the predicted chemical shifts for the F-state ensemble at 2.1 M GuHCl activity assuming a linear extrapolation of the predenaturation chemical shift changes. This takes into account the predenaturation chemical shift movements within the folded state ensemble and provides a better indication of the native to denatured state ensemble chemical shift changes.

precludes a fully quantitative evaluation. This is consistent with the rapid interchange of conformations that gives rise to the averaging of the NMR chemical shifts of the different conformers and is also consistent with the absence of hydrogen exchange protection in the 125−146 region of the protein.

Structure within the Denatured State of Prion Protein. On the high denaturant concentration side of the major unfolding transition of HuPrP, a denaturant-dependent loss of a residual far-UV CD response and an increase in molecular volume have been identified for the denatured state ensemble (*13*, *22*). The residual structure present in the denatured state ensemble is apposite, given the denaturing conditions used to generate putative synthetic prion infectivity (*13*).

To assess the conformational properties of the denatured state ensemble, a full backbone and C^{β} assignment was obtained for denatured PrP^{91-231} in 2.6 M GuHCl activity ([4.0 M GuHCl]). The chemical shift differences for C^{α} and C' resonances (Figure 3a,b) between the native and denatured state ensembles (0.0 vs 2.6 M GuHCl activity) illustrate the expected strong correlation with the backbone torsional angle distribution (and thus the backbone secondary structure content) of the native state (*44*, *45*). The chemical shifts of the C^{α} and carbonyl resonances in 2.6 M GuHCl activity are broadly within the ranges previously reported for random coils (*46*).

Changes in the Unfolded State Ensemble Changes. Despite the above, chemical shift changes of ^{15}N resonances over the range 2.1−3.4 M GuHCl activity ([3.0−6.4 M GuHCl]) indicate that the denatured state ensemble is changing markedly in conformational distribution as the denaturant concentration is increased (Figures 4 and 5).

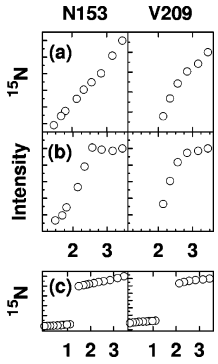

FIGURE 5: Behavior of representative ^{1}H−^{15}N HSQC peaks as a function of GuHCl activity. Data obtained from residues N153 and V209 are shown. (a) and (b) show changes in the denatured state ensemble as a function of GuHCl activity (M); (a) shows the change in ^{15}N chemical shift (ppm) and (b) shows the change of intensity. In the case of V209, the rapid loss of peak intensity at lower denaturant concentrations precluded measurement of data below 2.1 M GuHCl activity. (c) shows changes in ^{15}N chemical shift of the folded (<1.5 M GuHCl) and unfolded state ensembles (>1.5 M GuHCl) as a function of GuHCl activity.

The denaturant dependence of the population of this residual structure is low, indicating that this is not associated with a large-scale burial of hydrophobic groups, and is detectable over a wide range of denaturant concentrations (Figure 5a). Between 2.6 and 3.4 M GuHCl activity ([3.9−6.4 M GuHCl]), the population of the native state ensemble is less than 0.1% (as estimated from far-UV CD), but chemical shift changes of greater than 10% of the denatured state to native state transition occur (Figure 4a,c). These changes equate approximately with the amount of residual ellipticity observed from the denatured state ensemble (∼10%) (at ∼2.2M GuHCl activity) (*22*) and are consistent with the reduced hydrodynamic volume reported for denatured prion protein at elevated denaturant concentrations compared with that expected for the fully unfolded protein (*13*).

For much of the region that is structured within the native state ensemble, the sign and distribution of the chemical shift changes within the denatured state ensemble (Figure 4b,c) indicate that most of the residues that adopt α-helical conformations in the native structure are also helical in the denatured state ensemble. This conclusion is supported by ^{13}C chemical shift data which confirm that the ^{15}N chemical shift data provide an accurate indication of the protein secondary structure (data not shown) (*47*). This tendency to be in a nativelike conformation also applies to the second strand of the β-sheet, though to a lesser extent. However, the region corresponding to the first strand of the β-sheet in the native state ensemble shows less evidence of being nativelike, as does the loop linking this strand and helix I and the loop connecting helices II and III (Figure 4).

Together, this points to the distribution of species in the denatured state ensemble containing a sizable population that has conformations reflecting the native state backbone torsions, but which is expanded. Assuming the generally observed linear dependence of the free energy change (*36*) associated with this residual structure in the denatured state, in the absence of denaturant the proportion having a backbone conformation that resembles the native state would be at least 50% (Figure 5c).

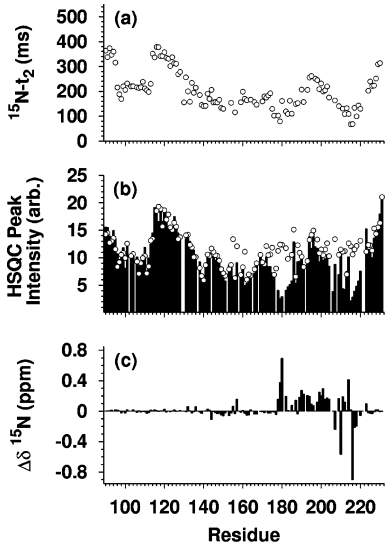

FIGURE 6: Dynamics of the denatured state ensemble and the effect of the prion protein disulfide bond. (a) ^{15}N T_2 relaxation rates of the denatured state ensemble at 3.4 M GuHCl activity ([6.4 M GuHCl]). (b) Filled bars show the intensity of HSQC peaks of prion protein with an intact disulfide bond also at 3.4 M GuHCl activity (arbitrary intensities). Open circles show the intensities following reduction of the disulfide bond. (c) shows ^{15}N chemical shift changes in backbone amide groups at 3.4 M GuHCl activity following reduction of the disulfide bond.

Intensity Changes within the Denatured State Ensemble. In line with the chemical shift changes, changes in the relaxation properties of nuclei within the denatured state ensemble of HuPrP indicate the population of partially structured species. Changes in the conformational distribution of the denatured state ensemble are reflected in the intensity of cross-peaks in ^{1}H$-^{15}$N HSQC spectra as a function of denaturant concentration (Figures 5b and 6b). Even at the highest denaturant concentration used here, 3.4 M GuHCl activity ([6.4 M GuHCl]), residues that make up much of the structured domain in the native state have significantly reduced signal intensities compared with other regions of the protein (Figure 6b). This is similarly shown by the individual ^{15}N relaxation rates of the denatured state ensemble at 3.4 M GuHCl activity (Figure 6a). Broadening of NMR signals, resulting in less intense peaks, can arise in heterogeneous systems due to insufficient time averaging of sampled chemical shifts, because of restricted mobility (typically because of conformational fluctuations on a millisecond to microsecond time scale). This is the so-called intermediate exchange regime (*48*). The regions that experience the greatest attenuation of intensity include those corresponding to the second strand of the β-sheet and helices II and III. In line with the chemical shift data, the regions preceding helix I in the native state ensemble (residues 115−146) and to the C-terminal region (residues 226−231) are less affected.

There is also a clear but less dramatic reduction in intensity in the N-terminal region (residues 93−114) in the denatured ensemble (Figure 6b). This region of the protein is unstructured in the native state of the protein and contains a high-affinity transition metal binding site (*49*, *50*). Intriguingly, this reduction in peak intensity appears to be due to this region of the protein exchanging between presumably more structured or collapsed species within the denatured state ensemble, rather than due to the presence of paramagnetic metal ions, as the addition of the metal chelator EDTA fails to result in the recovery of signal in this region of the protein (data not shown).

The observation of a residual contribution of more structured species to the resonance intensities at very high denaturant concentrations is consistent with the relatively low denaturant dependence of the population of these species within the denatured state ensemble, as reported by changes in chemical shift changes, far-UV CD, and hydrodynamic properties (Figures 5a,c and 1b) (*13*). The decrease in ^{1}H$-^{15}$N HSQC cross-peak intensities as the denaturant concentration is reduced over the range 3.4−2.6 M GuHCl activity ([6.4−3.9M GuHCl]) mirrors the other methods, but the nonlinearity of the resonance intensity with population makes quantification of the slope unachievable (Figure 5b).

However, at lower denaturant concentrations [in the range 2.6−2.1 M GuHCl activity for example ([3.9−3.0 M GuHCl])], the reduction in the intensity of cross-peaks in ^{1}H$-^{15}$N HSQC spectra is noticeably more severe. For some residues, attenuation of peak intensities at lower denaturant concentrations results in measurable decreases of intensity of over 8-fold between narrow denaturant concentration ranges (e.g., K194). This rate of loss of signal intensity is sufficient to render a number of resonances (32) below the limit of detection at 2.1 M GuHCl activity (Figure 4b). There was no substantial correlation observed between the reduction of NMR resonance intensities and the chemical shift differences (^{1}H chemical shift, ^{15}N chemical shift, or the modulus of ^{1}H and ^{15}N chemical shift difference) between the folded and denatured ensembles, indicating that the observed loss of peak intensities in this range of GuHCl concentration cannot be attributed solely to interconversion between the denatured and folded states. Instead, the loss of NMR signal intensity again reflects the increased population of a structured intermediate state within the denatured state ensemble. This loss of signal, resulting from resonance line broadening, is a common feature of highly collapsed, partially folded but non-native states, including the acid-denatured (molten globule) state of α-lactalbumin (*51*−*54*). Lack of fixed tertiary interactions in these states results in a fluctuating ensemble of structures, which interconvert on a millisecond to microsecond time scale.

Relationship of Persistent Structure to Disulfide Bond. Residues that are most susceptible to the reduction of signal intensities at lower denaturant concentrations (176−184, 214−218) are clustered around the disulfide bond, the so-called "hyperstable" region of the protein that is most resistant to hydrogen exchange (*22*, *23*) (Figure 6a), implying that this loss is due to increased population of a state containing this region. This observation is consistent with the relatively high denaturant dependence of the hydrogen exchange (*23*) for the hyperstable core, which means that its population is relatively small at high denaturant concentrations (>2.5 M GuHCl activity).

At elevated levels of denaturant, reduction of the disulfide bond results in the intensities of these residues recovering broadly to the level of the remainder of the C-terminus of the protein (Figure 6b). The regions of the protein affected by reduction of the disulfide bond are much more extensive than suggested by the hydrogen exchange data, encompassing the majority of helices II and III of native PrP^C (residues

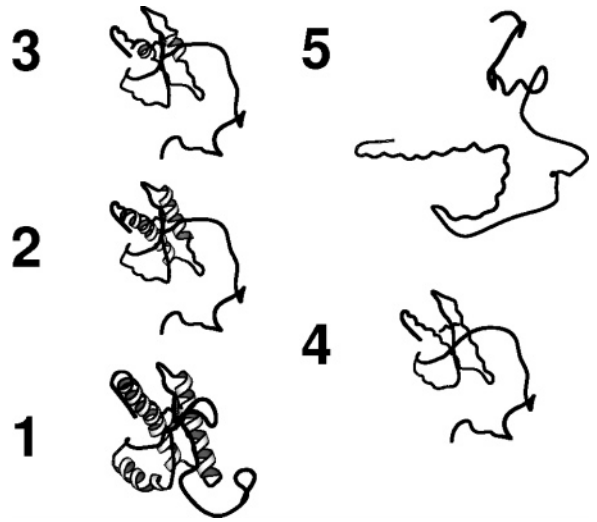

FIGURE 7: Schematic representation of secondary structure elements in the native (1), perturbed native (2), hyperstable-containing (3), molten globule (4), and unfolded (5) states of prion protein (PrP^{91-231}). This figure was created using MOLSCRIPT (*59*).

172−190 and 200−223, respectively). Indeed, changes in ^{15}N chemical shift (Figure 6c) indicate that the majority of residues beyond 180 are affected, further confirming the extensive nature of persistent structure within the denatured state ensemble.

It has been shown in a number of proteins that although disulfide bonds can constrain the unfolded state (*55*), their presence within collapsed structures can increase the extent of line broadening by generating additional barriers to conformational fluctuations (*52*). Restricted conformational exchange in these highly denatured states appears to be due to the inherent properties of the polypeptide chain. For example, the prion protein homologue, doppel, does not exhibit decreased hydrogen exchange around its two disulfide bonds (*23*).

DISCUSSION

In this study, we have used the denaturant concentration dependence of various NMR parameters to examine the folding transitions of PrP at equilibrium, to help understanding of the conversion of PrP^C to PrP^{Sc}. The behavior of HuPrP as a function of denaturant concentration provides evidence for at least five forms of the protein. Extrapolating the stability of these states to conditions where there is no denaturant present gives a free energy profile, as illustrated in Figure 7. The free energy values associated with each state are approximations since none of the transitions can be individually resolved. State 1 represents the native protein conformation present at neutral pH. State 2 is a perturbed native, where there is a conformational rearrangement or fraying of the C-termini of helices II and III and a perturbation of the loop connecting these helices. This is similar to the changes in the native state associated with the lowering of pH to 4.0 (*37*). Also in state 2, it appears that the N-terminal region of the folded domain (residues 125−146) spends a proportion of time detached from the remainder of the protein. This latter fluctuation leads to low protection against solvent amide hydrogen exchange and, most likely, the increase in hydrodynamic radius.

State 3 is a species with the hyperstable core identified by solvent hydrogen exchange from the native state. The extreme broadening of NMR resonances surrounding the disulfide bond appears to be due to restricted conformational exchange caused by the disulfide bond.

State 4 has the hallmarks of a molten globule species on the basis of NMR line width behavior and its hydrodynamic properties (*13*). In comparison to state 3, this state is a less folded species, containing nativelike conformational characteristics, with similar free energies to the fully expanded denatured protein. The structured region within this state encompasses the three helices and second strand of the β-sheet. State 5 is the fully unfolded random coil state.

Implications for the Study of Prion Protein Folding. One school of thought on the nature of unfolded states in proteins is that there is much residual nativelike secondary structure. The existence of this structure reduces the conformational search required to establish the native state and dominates the folding process (*52*, *56*, *57*). Given the strong correlation between secondary structure elements within the prion protein native state and structured elements within the prion protein intermediate state, it appears that the folding of oxidized prion protein may be strongly guided by nativelike conformational propensity in the denatured state. The data presented here are consistent with residual structure in the denatured state ensemble acting as a seed or template for the folding process, a factor that might explain the extremely fast folding rate of prion protein (*58*).

It is also interesting to note that the highly denaturing conditions in which this residual structure predominates are very similar to those conditions in which prion protein fibrils have been generated. Fibrils grown in these conditions have been reported to induce a prion-like disease in transgenic mice overexpressing a truncated PrP, and it is possible that such partially ordered or pre-molten globule states may the principal precursor in the formation of ordered fibrillar structures (*27*).

REFERENCES

1. Sipe, J. D., and Cohen, A. S. (2000) Review: history of the amyloid fibril, *J. Struct. Biol. 130*, 88−98.
2. McKinley, M. P., Bolton, D. C., and Prusiner, S. B. (1983) A protease-resistant protein is a structural component of the scrapie prion, *Cell 35*, 57−62.
3. Collinge, J. (2001) Prion diseases of humans and animals: their causes and molecular basis, *Annu. Rev. Neurosci. 24*, 519−550.
4. Prusiner, S. B. (1998) Prions, *Proc. Natl. Acad. Sci. U.S.A. 95*, 13363−13383.
5. Griffith, J. S. (1967) Self-replication and scrapie, *Nature 215*, 1043−1044.
6. Prusiner, S. B. (1982) Novel proteinaceous infectious particles cause scrapie, *Science 216*, 136−144.
7. Booth, D. R., Sunde, M., Bellotti, V., Robinson, C. V., Hutchinson, W. L., Fraser, P. E., Hawkins, P. N., Dobson, C. M., Radford, S. E., Blake, C. C. F., and Pepys, M. B. (1997) Instability, unfolding and aggregation of human lysozyme variants underlying amyloid fibrillogenesis, *Nature 385*, 787−793.
8. Hammarstrom, P., Jiang, X., Hurshman, A. R., Powers, E. T., and Kelly, J. W. (2002) Sequence-dependent denaturation energetics: A major determinant in amyloid disease diversity, *Proc. Natl. Acad. Sci. U.S.A. 99* (Suppl. 4), 16427−16432.
9. Ramirez-Alvarado, M., Merkel, J. S., and Regan, L. (2000) A systematic exploration of the influence of the protein stability on amyloid fibril formation in vitro, *Proc. Natl. Acad. Sci. U.S.A. 97*, 8979−8984.
10. Smith, D. P., Jones, S., Serpell, L. C., Sunde, M., and Radford, S. E. (2003) A systematic investigation into the effect of protein

destabilisation on beta 2-microglobulin amyloid formation, *J. Mol. Biol. 330*, 943−954.
11. Liemann, S., and Glockshuber, R. (1999) Influence of amino acid substitutions related to inherited human prion diseases on the thermodynamic stability of the cellular prion protein, *Biochemistry 38*, 3258−3267.
12. Nandi, P. K., Leclerc, E., Nicole, J. C., and Takahashi, M. (2002) DNA-induced partial unfolding of prion protein leads to its polymerisation to amyloid, *J. Mol. Biol. 322*, 153−161.
13. Baskakov, I. V., Legname, G., Gryczynski, Z., and Prusiner, S. B. (2004) The peculiar nature of unfolding of the human prion protein, *Protein Sci. 13*, 586−595.
14. Legname, G., Baskakov, I. V., Nguyen, H. O., Riesner, D., Cohen, F. E., DeArmond, S. J., and Prusiner, S. B. (2004) Synthetic mammalian prions, *Science 305*, 673−676.
15. Riek, R., Hornemann, S., Wider, G., Billeter, M., Glockshuber, R., and Wuthrich, K. (1996) NMR structure of the mouse prion protein domain PrP (121−231), *Nature 382*, 180−182.
16. Hosszu, L. L. P., Jackson, G. S., Trevitt, C. R., Jones, S., Batchelor, M., Bhelt, D., Prodromidou, K., Clarke, A. R., Waltho, J. P., and Collinge, J. (2004) The residue 129 polymorphism in human prion protein does not confer susceptibility to CJD by altering the structure or global stability of PrPC, *J. Biol. Chem. 279*, 28515−28521.
17. Jackson, G. S., Hosszu, L. L. P., Power, A., Hill, A. F., Kenney, J., Saibil, H., Craven, C. J., Waltho, J. P., Clarke, A. R., and Collinge, J. (1999) Reversible conversion of monomeric human prion protein between native and fibrilogenic conformations, *Science 283*, 1935−1937.
18. Hornemann, S., and Glockshuber, R. (1998) A scrapie-like unfolding intermediate of the prion protein domain PrP(121−231) induced by acidic pH, *Proc. Natl. Acad. Sci. U.S.A. 95*, 6010−6014.
19. Swietnicki, W., Petersen, R., Gambetti, P., and Surewicz, W. K. (1997) pH-dependent stability and conformation of the recombinant human prion protein PrP(90−231), *J. Biol. Chem. 272*, 27517−27520.
20. Baskakov, I. V., Legname, G., Baldwin, M. A., Prusiner, S. B., and Cohen, F. E. (2002) Pathway complexity of prion protein assembly into amyloid, *J. Biol. Chem. 277*, 21140−21148.
21. Morillas, M., Vanik, D. L., and Surewicz, W. K. (2001) On the mechanism of α-helix to β-sheet transition in the recombinant prion protein, *Biochemistry 40*, 6982−6987.
22. Hosszu, L. L. P., Baxter, N. J., Jackson, G. S., Power, A., Clarke, A. R., Waltho, J. P., Craven, C. J., and Collinge, J. (1999) Structural mobility of the human prion protein probed by backbone hydrogen exchange, *Nat. Struct. Biol. 6*, 740−743.
23. Nicholson, E. M., Mo, H., Prusiner, S. B., Cohen, F. E., and Marqusee, S. (2002) Differences between the prion protein and its homolog Doppel: a partially structured state with implications for scrapie formation, *J. Mol. Biol. 316*, 807−815.
24. Huyghues-Despointes, B. M., Scholtz, J. M., and Pace, C. N. (1999) Protein conformational stabilities can be determined from hydrogen exchange rates, *Nat. Struct. Biol. 6*, 910−912.
25. Last, A. M., Schulman, B. A., Robinson, C. V., and Redfield, C. (2001) Probing subtle differences in the hydrogen exchange behavior of variants of the human alpha-lactalbumin molten globule using mass spectrometry, *J. Mol. Biol. 311*, 909−919.
26. Yokota, A., Hirai, K., Miyauchi, H., Iimura, S., Noda, Y., Inoue, K., Akasaka, K., Tachibana, H., and Segawa, S. (2004) NMR characterization of three-disulfide variants of lysozyme, C64A/C80A, C76A/C94A, and C30A/C115A—a marginally stable state in folded proteins, *Biochemistry 43*, 6663−6669.
27. Uversky, V. N., and Fink, A. L. (2004) Conformational constraints for amyloid fibrillation: the importance of being unfolded, *Biochim. Biophys. Acta 1698*, 131−153.
28. Johnson, B. A., and Blevins, R. A. (1994) NMR view—A computer-program for the visualization and analysis of NMR data, *J. Biomol. NMR 4*, 603−614.
29. Bax, A., and Ikura, M. (1991) An efficient 3D NMR technique for correlating the proton and ^{15}N backbone amide resonances with the alpha-carbon of the preceding residue in uniformly ^{15}N/^{13}C enriched proteins, *J. Biomol. NMR 1*, 99−104.
30. Wittekind, M., and Mueller, L. (1993) HNCACB, a high-sensitivity 3D NMR experiment to correlate amide-proton and nitrogen resonances with the alpha-carbon and beta-carbon resonances in proteins, *J. Magn. Reson., Ser. B 101*, 201−205.
31. Muhandiram, D. R., and Kay, L. E. (1994) Gradient-enhanced triple-resonance 3-dimensional NMR experiments with improved sensitivity, *J. Magn. Reson., Ser. B 103*, 203−216.
32. Kay, L. E., Xu, G. Y., and Yamazaki, T. (1994) Enhanced-sensitivity triple-resonance spectroscopy with minimal H20 saturation, *J. Magn. Reson., Ser. A 109*, 129−133.
33. Reed, M. A., Hounslow, A. M., Sze, K. H., Barsukov, I. G., Hosszu, L. L., Clarke, A. R., Craven, C. J., and Waltho, J. P. (2003) Effects of domain dissection on the folding and stability of the 43 kDa protein PGK probed by NMR, *J. Mol. Biol. 330*, 1189−1201.
34. Bodenhausen, G., and Ruben, D. J. (1980) Natural abundance N-15 NMR by enhanced heteronuclear spectroscopy, *Chem. Phys. Lett. 69*, 185−189.
35. Schleucher, J., Schwendinger, M., Sattler, M., Schmidt, P., Schedletzky, O., Glaser, S. J., Sorensen, O. W., and Griesinger, C. (1994) A general enhancement scheme in heteronuclear multidimensional NMR employing pulsed field gradients, *J. Biomol. NMR 4*, 301−306.
36. Parker, M. J., Spencer, J., and Clarke, A. R. (1995) An integrated kinetic analysis of intermediates and transition states in protein folding reactions, *J. Mol. Biol. 253*, 771−786.
37. Calzolai, L., and Zahn, R. (2003) Influence of pH on NMR structure and stability of the human prion protein globular domain, *J. Biol. Chem 278*, 35592−35596.
38. Knaus, K. J., Morillas, M., Swietnicki, W., Malone, M., Surewicz, W. K., and Yee, V. C. (2001) Crystal structure of the human prion protein reveals a mechanism for oligomerization, *Nat. Struct. Biol. 8*, 770−774.
39. Staniforth, R. A., Giannini, S., Higgins, L. D., Conroy, M. J., Hounslow, A. M., Jerala, R., Craven, C. J., and Waltho, J. P. (2001) Three-dimensional domain swapping in the folded and molten-globule states of cystatins, an amyloid-forming structural superfamily, *EMBO J. 20*, 4774−4781.
40. Jerala, R., and Zerovnik, E. (1999) Accessing the global minimum conformation of stefin A dimer by annealing under partially denaturing conditions, *J. Mol. Biol. 291*, 1079−1089.
41. Sokolowski, F., Modler, A. J., Masuch, R., Zirwer, D., Baier, M., Lutsch, G., Moss, D. A., Gast, K., and Naumann, D. (2003) Formation of critical oligomers is a key event during conformational transition of recombinant syrian hamster prion protein, *J. Biol. Chem. 278*, 40481−40492.
42. Kuwata, K., Li, H., Yamada, H., Legname, G., Prusiner, S. B., Akasaka, K., and James, T. L. (2002) Locally disordered conformer of the hamster prion protein: a crucial intermediate to PrP(Sc)?, *Biochemistry 41*, 12277−12283.
43. Torrent, J., Alvarez-Martinez, M. T., Liautard, J. P., Balny, C., and Lange, R. (2005) The role of the 132−160 region in prion protein conformational transitions, *Protein Sci. 14*, 956−967.
44. Wishart, D. S., Sykes, B. D., and Richards, F. M. (1992) The chemical shift index: a fast and simple method for the assignment of protein secondary structure through NMR spectroscopy, *Biochemistry 31*, 1647−1651.
45. Cornilescu, G., Delaglio, F., and Bax, A. (1999) Protein backbone angle restraints from searching a database for chemical shift and sequence homology, *J. Biomol. NMR 13*, 289−302.
46. Wishart, D. S., Bigam, C. G., Yao, J., Abildgaard, F., Dyson, H. J., Oldfield, E., Markley, J. L., and Sykes, B. D. (1995) H-1, C-13 and N-15 chemical-shift referencing in biomolecular NMR, *J. Biomol. NMR 6*, 135−140.
47. Reed, M. A., Jelinska, C., Syson, K., Splevins, A., Alizadeh, T., Hounslow, A. M., Staniforth, R. A., Clarke, A. R., Craven, C. J., and Waltho, J. P. (2005) Non native-like topology in a denatured protein (submitted for publication).
48. Homans, S. W. (1989) *A Dictionary of Concepts in NMR*, Oxford University Press, Oxford, U.K.
49. Jackson, G. S., Murray, I., Hosszu, L. L. P., Gibbs, N., Waltho, J. P., Clarke, A. R., and Collinge, J. (2001) Location and properties of metal-binding sites on the human prion protein, *Proc. Natl. Acad. Sci. U.S.A. 98*, 8531−8535.
50. Wells, M. A., Jackson, G. S., Jones, S., Hosszu, L. L., Craven, C. J., Clarke, A. R., Collinge, J., and Waltho, J. P. (2005) Copper II mediates communication between the octapeptide repeats and the minimal replicating unit of human prion protein (submitted for publication).
51. Redfield, C., Schulman, B. A., Milhollen, M. A., Kim, P. S., and Dobson, C. M. (1999) Alpha-lactalbumin forms a compact molten

globule in the absence of disulfide bonds, *Nat. Struct. Biol. 6*, 948−952.

52. Schulman, B. A., Kim, P. S., Dobson, C. M., and Redfield, C. (1997) A residue-specific NMR view of the non-cooperative unfolding of a molten globule, *Nat. Struct. Biol. 4*, 630−634.
53. Wang, Y., Alexandrescu, A. T., and Shortle, D. (1995) Initial studies of the equilibrium folding pathway of staphylococcal nuclease, *Philos. Trans. R. Soc. London, Ser. B: Biol. Sci. 348*, 27−34.
54. Redfield, C. (2004) NMR studies of partially folded molten-globule states, *Methods Mol. Biol. 278*, 233−254.
55. Clarke, J., Hounslow, A. M., Bond, C. J., Fersht, A. R., and Daggett, V. (2000) The effects of disulfide bonds on the denatured state of barnase, *Protein Sci. 9*, 2394−2404.
56. Shortle, D., and Ackerman, M. S. (2001) Persistence of native-like topology in a denatured protein in 8 M urea, *Science 293*, 487−489.
57. Klein-Seetharaman, J., Oikawa, M., Grimshaw, S. B., Wirmer, J., Duchardt, E., Ueda, T., Imoto, T., Smith, L. J., Dobson, C. M., and Schwalbe, H. (2002) Long-range interactions within a nonnative protein, *Science 295*, 1719−1722.
58. Wildegger, G., Liemann, S., and Glockshuber, R. (1999) Extremely rapid folding of the C-terminal domain of the prion protein without kinetic intermediates, *Nat. Struct. Biol. 6*, 550−553.
59. Kraulis, P. J. (1991) MOLSCRIPT—A program to produce both detailed and schematic plots of protein structures, *J. Appl. Crystallogr. 24*, 946−950.

BI051277K